Magnetodielectric coupling of infrared phonons in single-crystal Cu_2OSeO_3

K. H. Miller,[1] X. S. Xu.,[2] H. Berger,[3] E. S. Knowles,[1] D. J. Arenas,[1,4] M. W. Meisel,[1] and D. B. Tanner[1]
[1]*Department of Physics, University of Florida, Gainesville, Florida 32611-8440, USA*
[2]*Materials Science and Technology Division, Oak Ridge National Laboratory, Oak Ridge, Tennessee 37831, USA*
[3]*Institute of Physics of Complex Matter, Ecole Polytechnique Federal de Lausanne, CH-1015 Lausanne, Switzerland*
[4]*Department of Physics, University of North Florida, Jacksonville, Florida 32224, USA*
(Received 21 June 2010; revised manuscript received 2 September 2010; published 15 October 2010)

Reflection and transmission as a function of temperature (5–300 K) have been measured on a single crystal of the magnetoelectric ferrimagnetic compound Cu_2OSeO_3 utilizing light spanning the far infrared to the visible portions of the electromagnetic spectrum. The complex dielectric function and optical properties were obtained via Kramers-Kronig analysis and by fits to a Drude-Lortentz model. The fits of the infrared phonons show a magnetodielectric effect near the transition temperature ($T_c \sim 60$ K). Assignments to strong far-infrared phonon modes have been made, especially those exhibiting anomalous behavior around the transition temperature.

DOI: 10.1103/PhysRevB.82.144107 PACS number(s): 78.30.−j, 78.20.−e

I. INTRODUCTION

The magnetodielectric effect refers to a change in the dielectric constant induced by an external magnetic field or by the onset of spontaneous magnetization. Observable anomalies in the polarization of a material near a magnetic transition indicate the presence of finite magnetoelectric coupling, i.e., a cross coupling between magnetic and electric orders. Magnetoelectric coupling has attracted significant interest[1–3] recently not only for scientific purposes but also for its use in novel technological devices. One can envision field sensors and magnetic memory switches where the magnetic order could be altered by adjusting the electric field. A shortcoming of magnetoelectrics has been the scarcity of materials that can simultaneously support magnetic and electric orders. The fundamental issue behind this scarcity does not lie in the symmetry demands of the two orders; rather, the particular electron configurations that favor their origins are of a contradictory nature.[4] The electron configurations required by magnetism usually prevail and the electric ordering is forced to originate from "improper" means.[5] Recent studies on materials such as $TbMn_2O_5$,[6] $DyMn_2O_5$,[7] and $BiMnO_3$ (Ref. 8) all show magnetodielectric effects near magnetic transition temperatures where a distortion of the unit cell is also observed, as required by magnetic ordering. This evidence suggests that the change in lattice constant, which results in a corresponding change in bond lengths, is the mechanism that alters the polarity at T_c and, hence, produces a dielectric anomaly.

Here we report our infrared studies on a single crystal of Cu_2OSeO_3, a piezoelectric with a ferrimagnetic transition temperature of $T_c \sim 60$ K.[9] A previous study on Cu_2OSeO_3 by Bos *et al.*[9] reported a magnetodielectric effect (anomalous jump in dielectric constant) at the ferrimagnetic transition temperature, as observed through dielectric capacitance measurements. Although we found no drastic anomalies across T_c, a thorough inspection of the data combined with some modeling lead us to a magnetodielectric effect as well. Recently Gnezdilov *et al.*[10] have presented a Raman study of Cu_2OSeO_3 prepared in the same way as our crystal. They observed the abrupt appearance of three new lines in the spectra upon cooling below T_c, and an additional two lines that appeared below 20 K. Gnezdilov *et al.* also gave a detailed description of the crystal and magnetic symmetries of this compound.

Effenberger and Pertlik[11] solved the crystal structure using single-crystal x-ray diffraction. The compact crystal structure consists of three basic building blocks, square pyramidal CuO_5, trigonal bipyramidal CuO_5, and a lone pair containing tetrahedral SeO_3 unit. The oxygen atoms in the unit cell are shared among the three building blocks. The square pyramidal CuO_5 units exist in a 3-to-1 ratio to the trigonal bipyramidal CuO_5 units within the conventional unit cell. This ratio will be important subsequently when explaining the magnetic structure. All copper ions possess a +2 oxidation state. More detailed descriptions of the crystal structure are found elsewhere.[9,12]

The material crystallizes in the $P2_13$ cubic space group and has been shown to remain metrically cubic with no abnormal change in the lattice constant through the Curie temperature and down to 10 K.[9] The onset of magnetic order does have the effect of reducing the crystal symmetry to R3. Full cubic symmetry would require all copper ions to feel the same Coulomb interaction from nearest-neighbor copper spins. The proceeding explanation is the case for ferromagnetism and antiferromagnetism but not for ferrimagnetism, which is why a reduction from cubic symmetry must accompany this ordering.

II. EXPERIMENTAL PROCEDURES

Single crystals of Cu_2OSeO_3 were grown by a standard chemical vapor phase method. Mixtures of high-purity CuO (Alfa-Aesar, 99.995%) and SeO_2 (Alfa-Aesar, 99.999%) powder in molar ratio 2:1 were sealed in quartz tubes with electronic grade HCl as the transport gas for the crystal growth. The ampoules were then placed horizontally into a tubular two-zone furnace and heated slowly by 50 °C/h to 600 °C. The optimum temperatures at the source and deposition zones for the growth of single crystals have been

found to be 610 °C and 500 °C, respectively. After 6 weeks, many dark green, indeed almost black, Cu_2OSeO_3 crystals with a maximum size of $8\times6\times3$ mm^3 were obtained. X-ray powder diffraction analysis was conducted on a Rigaku x-ray diffractometer with Cu $K\alpha$ radiation (λ =1.5418 Å). An electron microprobe was used for chemical analysis of all solid samples.

The temperature-dependent (5–300 K) reflectance and transmittance measurements employed a Bruker 113v Fourier transform interferometer in conjunction with a helium-cooled silicon bolometer detector in the spectral range 30–700 cm^{-1} and with a nitrogen-cooled MCT detector from 700–5000 cm^{-1}. Room-temperature measurements from 5000–40 000 cm^{-1} were obtained with a Zeiss microscope photometer. After measuring the bulk reflectance over the entire spectral range, a crystal was polished to a thickness of 194 μm for transmittance measurements. All measurements were performed using unpolarized light at near-normal incidence with the electric field of the light in the ⟨111⟩ crystal plane. The cubic nature of the material forbids anisotropy in the optical spectra. Magnetic measurements were performed in a commercial superconducting quantum interference device magnetometer on a single-crystal sample mounted with the [111] axis parallel to the applied field. After cooling the sample in zero field to 50 K, magnetization was measured in an applied field of 10 G while warming to 70 K. The dc susceptibility was calculated in the low-field limit as $\chi(T)=M(T)/H$. In addition, the isothermal magnetization as a function of applied field was measured at a temperature of 2 K while sweeping the field from 0 to 2 kG and back to 0.

III. RESULTS AND ANALYSIS

A. Magnetism

Recent studies have measured the magnetic susceptibility of powdered samples Cu_2OSeO_3, finding ordering temperatures of $T_c^{\text{inflection}}=55$ K (Ref. 13) and $T_c^{\text{onset}}=60$ K.[9] Because anomalies in the infrared spectrum at the transition temperature are important, an accurate determination of T_c for the single crystal of interest was desired. The measured dc susceptibility as a function of temperature, $\chi(T)$, is shown in Fig. 1. Taking the transition temperature to be where the susceptibility turns upward, $T_c^{\text{onset}}=60$ K is found, consistent with the observations of Bos *et al.*[9] At 2 K (Fig. 1 inset), well within the ordered state, the magnetization saturates in a field of 800 G at $1.0N\mu_B$, which is half of the expected saturation value for a $S=1/2$ system, indicating a ferrimagnetic ordering in a three-up and one-down configuration. This three-up, one-down configuration of the $Cu2^+$ spins on the ordered state is also observed in a recent NMR study on the same Cu_2OSeO_3 single crystal compound.[17] No coercive field was measured; however, an inflection point with some slight hysteresis was observed near 400 G, which is also consistent with the findings of Bos *et al.*[9]

B. Reflectance and transmittance spectra

The temperature-dependent reflectance spectrum of Cu_2OSeO_3 between 30 and 1000 cm^{-1} (4–120 meV) is shown in Fig. 2. A strong sharpening of many phonon modes is observed with decreasing temperature. It should be noted that there are no drastic anomalies in the far-infrared spectrum, such as the presence of new modes or the splitting of existing modes. Because infrared spectroscopy is extremely sensitive to changes in dipole moments and force constants, the absence of these anomalies gives strong support to the assertion of no lattice distortions at T_c as initially determined by x-ray diffraction measurements.[9]

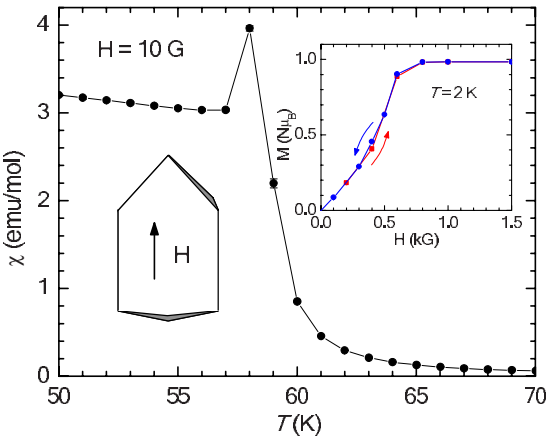

FIG. 1. (Color online) The dc susceptibility, $\chi(T)$, of Cu_2OSeO_3 near the ordering temperature (T_c=60 K) in an applied field of 10 G as measured while warming after zero-field cooling to 50 K. The inset shows the isothermal magnetization, $M(H)$, as a function of applied field at 2 K, where the field was swept up to 2 kG before being reduced to zero. In all instances, the lines connecting the data points are guides for the eyes. The schematic shows the orientation of the single crystal with respect to the field applied parallel to the [111] direction.

The top panel of Fig. 3 shows the 300 K reflectance up to 40 000 cm^{-1}. The onset of electronic absorption is indicated by the upturn around 26 000 cm^{-1} (3.2 eV). The transmittance spectra, as depicted in Fig. 4, are in good agreement with the reflectance measurements. At frequencies below the strong phonon modes (<80 cm^{-1}), the crystal transmits. The

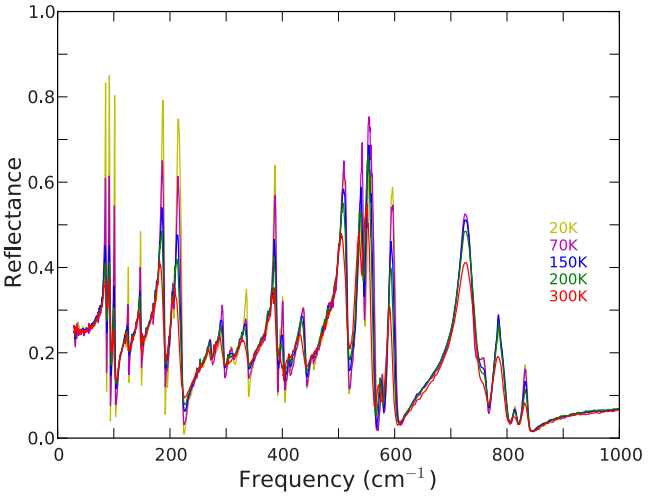

FIG. 2. (Color online) Temperature-dependent reflectance spectrum of Cu_2OSeO_3.

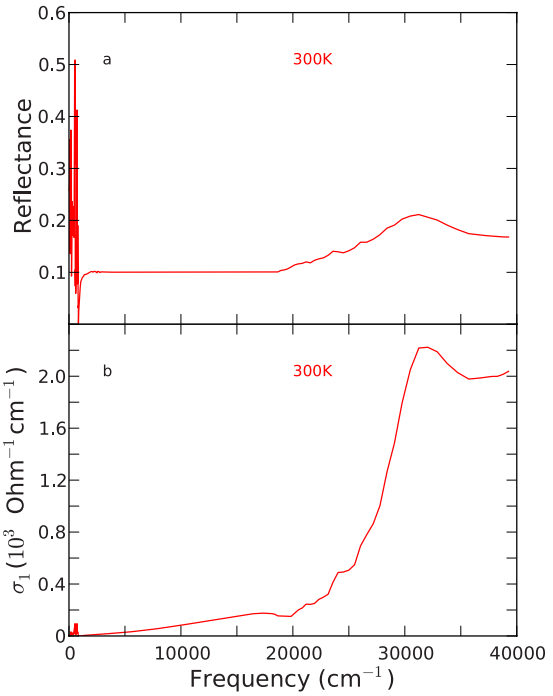

FIG. 3. (Color online) The upper panel (a) shows the 300 K broadband reflectance out to 40 000 cm^{-1}. The lower panel (b) depicts the optical conductivity at room temperature over the same frequency region.

periodic oscillations in this range are the Fabry-Perot interference fringes due to multiple internal reflections. Transmission gaps open between the infrared phonon modes. These regions become increasingly more evident as temperature is lowered and the modes sharpen. The low-frequency transmission spectrum exhibits a weak phonon with a resonance frequency of 68 cm^{-1} that first appears as a small structure around 120 K and strengthens with decreasing temperature.

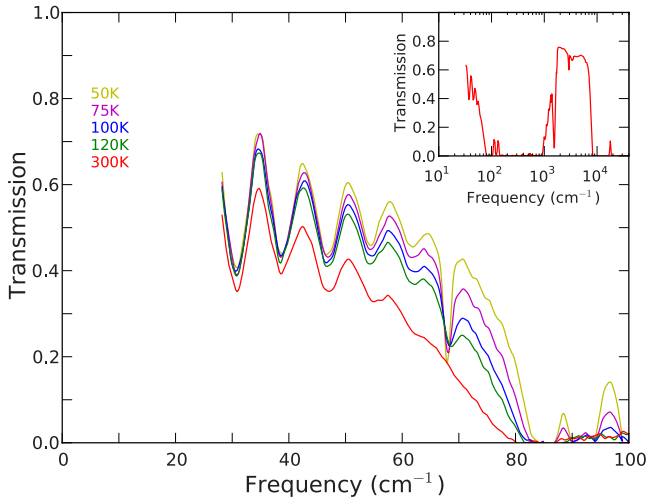

FIG. 4. (Color online) Temperature-dependent transmission spectrum of 194-μm-thick Cu_2OSeO_3 single crystal below 100 cm^{-1}. This region is highlighted by a weak phonon ($\sim$68 cm^{-1}) that begins to appear around 120 K. The inset shows transmission at 300 K measured out to the 40 000 cm^{-1}.

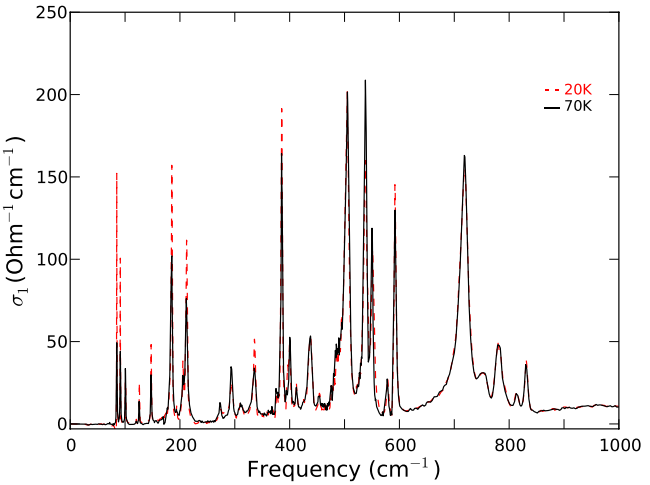

FIG. 5. (Color online) Far-infrared optical conductivity Cu_2OSeO_3 at 20 K (red, dashed line) 70 K (black, solid line).

The mode has a small oscillator strength, thus explaining why it was not observed in reflection. The weak phonon shows no response to a field of 0.14 kG parallel to the crystal surface; however, a magnetic origin for this structure cannot be ruled out and is worthy of future investigation. In contrast, the high-frequency spectra (inset Fig. 4) possesses two sharp dips, 1530 and 2054 cm^{-1}, which are too high to be single phonon peaks. Consequently, we are not able to make an assignment of these features.

C. Kramers-Kronig analysis and optical properties

Kramers-Kronig analysis can be used to estimate the real and imaginary parts of the dielectric function from the bulk reflectance $R(\omega)$.[14] Before calculating the Kramers-Kronig integral, the low-frequency data were extrapolated as a constant for $\omega \rightarrow 0$ as befits an insulator. At high frequencies the reflectance was assumed to be constant up to 1×10^7 cm^{-1}, after which $R \sim (\omega)^{-4}$ was assumed as the appropriate behav-

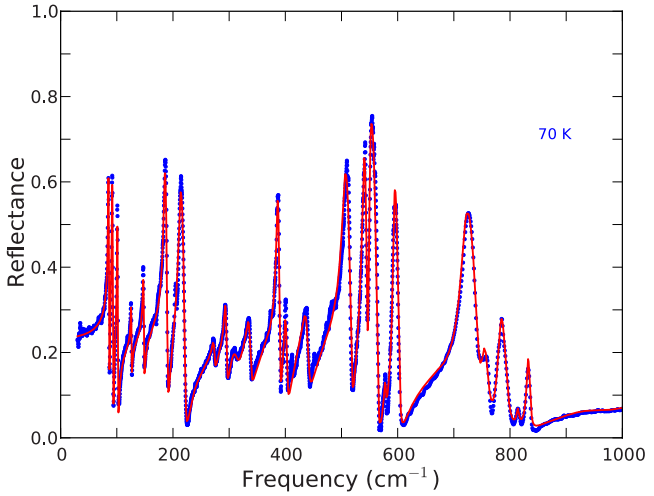

FIG. 6. (Color online) Experimental reflectance (blue points) and calculated reflectance (red line) from the Drude-Lorentz model of the Cu_2OSeO_3 70 K dielectric function.

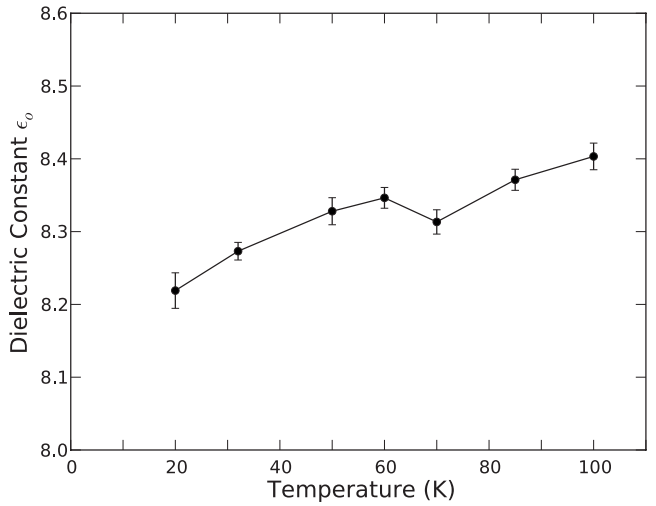

FIG. 7. The static dielectric constant as calculated from the Drude-Lorentz model at temperatures between 20 and 100 K, including T_c.

ior for free carriers. The optical properties were derived from the measured reflectance and the Kramers-Kronig-derived phase shift on reflection; in particular, we estimated the real part of the optical conductivity, $\sigma_1(\omega)$.

Figure 3(b) shows the optical conductivity at room temperature out to 40 000 cm^{-1}. The low absorption in the infrared is consistent with the insulating nature of the compound. Our temperature-dependent measurements ceased at 5000 cm^{-1}. Accordingly, the dynamics of interband transitions with temperature in the region of high photon energy do not contribute to our overall findings. Figure 5 depicts $\sigma_1(\omega)$ at 20 K (below T_c) and 70 K (above T_c) from 30 to 1000 cm^{-1}. The principal effect is a sharpening of most modes, yielding a larger conductivity at the resonant frequency.

The phonon modes in reflectance appear as Lorentzian lines in the optical conductivity, making them intuitive for modeling as harmonic oscillators. The vanishingly small static limit of $\sigma_1(\omega)$ and the low background level of conductivity throughout the infrared regions is further evidence of the insulating nature of the compound.

D. Oscillator-model fits

The Drude-Lorentz model was used to fit the reflectance and obtain a second estimate of the complex dielectric function in the infrared range. The model consists of a damped oscillator for each putative phonon in the spectrum plus a high-frequency permittivity ε_∞ that describes the contribution of all electronic excitations. The model has the following mathematical form:

$$\varepsilon = \sum_{j=1}^{\infty} \frac{S_j \omega_j^2}{\omega_j^2 - \omega^2 - i\omega\gamma_j} + \varepsilon_\infty, \tag{1}$$

where S_j, ω_j, and γ_j represent the oscillator strength, center frequency, and linewidth of the jth damped oscillator. The complex dielectric function provided by the Drude-Lorentz model is used to calculate the reflectivity, which agrees well with our original measured quantity. Figure 6 compares the calculated reflectivity and the measured reflectivity at 70 K. Similar quality fits were obtained at all other temperatures.

IV. DISCUSSION

A. Magnetodielectric effect

Equipped with oscillator parameters to describe each of the infrared phonons at all measured temperatures, one is now in position to closely monitor the subtle dynamics of the phonon structures across the transition temperature. Despite the lack of drastic changes in the phonon spectrum at T_c, it is worthwhile examining whether a combination of many small anomalies in the phonon dynamics might sum to give an overall effect. At this point it is logical to examine the static dielectric constant because it is the sum of parameters that describe the dielectric nature of the compound (the side to which the infrared is most sensitive). Taking the zero-

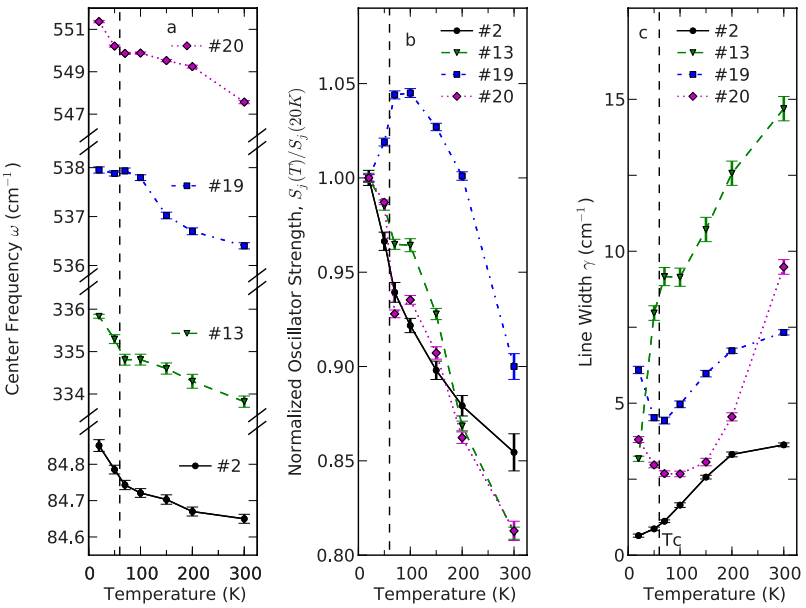

FIG. 8. (Color online) The (a) center frequency, (b) normalized oscillator strength, and (c) linewidth of four oscillators as a function of temperature. Oscillator #2 is a typical conventional phonon whereas the other three oscillators show anomalous behavior as temperature is lowered across T_c.

TABLE I. Oscillator parameters for Cu_2OSeO_3 (at 20 K) and their corresponding assignments for a few strong modes in the far infrared.

Index	Osc strength S	Center freq, ω (cm^{-1})	Linewidth, γ (cm^{-1})	Anomalous, type A, B, C, or No	Assignment
1	0.003	67.7	1.1	No	
2	0.501	84.9	0.6	No	Vibration of CuO_5 units
3	0.337	91.2	0.6	No	
4	0.233	100.7	0.5	No	
5	0.073	126.1	0.8	No	
6	0.134	147.5	1.2	Type A	
7	0.544	184.8	1.5	Type B	
8	0.071	204.8	2.4	Type C	
9	0.521	212.0	2.9	No	SeO_3 vibrating against CuO_5
10	0.038	273.9	5.5	Type C	
11	0.123	293.2	7.6	Type C	
12	0.042	311.7	6.2	Type B	
13	0.107	335.8	3.6	Type C	Internal in-plane vibration of CuO_5 units
14	0.188	385.5	2.0	No	Internal bending mode of SeO_3 units
15	0.063	399.4	3.6	No	
16	0.095	437.4	5.9	Type C	Internal out-of-plane vibration of CuO_5 units
17	0.007	454.1	4.3	No	
18	0.445	504.5	7.4	No	
19	0.224	537.9	6.5	Type C	
20	0.091	551.3	3.8	Type C	
21	0.094	592.5	3.4	Type C	
22	0.291	717.1	15.8	Type B	Antisymmetric stretch of SeO_3 units
23	0.024	753.1	11.6	No	
24	0.054	781.7	13.9	Type A	Antisymmetric stretch of SeO_3 units
25	0.017	813.8	6.6	No	
26	0.016	831.3	5.1	No	Radial breathing mode of SeO_3 units

frequency limit of the Drude-Lorentz formula, one arrives at the following simple expression for the static dielectric constant:

$$\varepsilon_o = \sum_{j=1}^{\infty} S_j + \varepsilon_\infty. \quad (2)$$

The calculated static dielectric constant at temperatures near T_c is shown in Fig. 7. There is an anomalous jump at 60 K. It should be noted that this magnetodielectric effect in Cu_2OSeO_3 was previously observed by Bos *et al.*[9] through dielectric capacitance measurements. While the value of the dielectric constant measured here is considerably smaller than that in the previous report, the direction and magnitude of the anomaly at T_c are in good agreement. It is also worthwhile to note that the systematic changes in reflectance near T_c over the midinfrared band (1000–5000 cm^{-1}) corresponded to changes in the midinfrared dielectric function that were one order of magnitude less than our magnetodielectric effect, thus identifying phonons as the main contributor to this effect.

B. Anomalous phonons

The observed phonons in Cu_2OSeO_3 may be divided into two categories: conventional and anomalous. Conventional phonons show a slight hardening of their frequencies when cooled to low temperatures, accompanied by a significant reduction in linewidth and at most modest changes in oscillator strength. Moreover, the temperature variation is smooth with no sudden changes in slope or value. Anomalous phonons violate one or more of these expectations. We have identified 13 anomalous phonons in our spectra, which show 26 total modes. A numbering scheme has been used which corresponds to the sequence of appearance of oscillators in the infrared spectrum starting with #1 (lowest frequency mode) and ending with #26 (highest frequency mode)

Figure 8[IN] displays the temperature dependence of the three oscillator parameters for three of the 13 anomalous phonons (#13, #19, and #20) in the infrared spectrum. The oscillator strength, represented by S_j, was calculated from the spectral weight and center frequency of each phonon using the relation $S_j=(\omega_{pj}/\omega_{oj})^2$. The behavior of S_j directly results from changes in ω_p. The oscillator parameters for one conventional phonon (#2) are shown for comparison. It was ob-

TABLE II. Center frequency and intensity of the 41 predicted infrared active modes in Cu_2OSeO_3.

Center freq, ω (cm^{-1})	Dipole moment (arb. units)	Experimentally observed, exp. index	Atomic motion description
87.1[a]	0.02		General motion[b] of CuO_5 units
89.9[a]	0.05		Vibration of CuO_5 units
92.5	0.16	2	Vibration of CuO_5 units
104.5	0.02		General motion of CuO_5 units
112.7	0.08		Vibration of CuO_5 trigonal bipyramidal against CuO_5 square pyramidal
114.3	0.13		Vibration of CuO_5 trigonal bipyramidal against CuO_5 square pyramidal
127.9[a]	0.05		General motion of CuO_5 units
130.8[a]	0.04		General motion of CuO_5 units
143.9	0.11		General motion of CuO_5 units
159.7[a]	0.03		General motion of CuO_5 units
173.8[a]	0.03		General motion of CuO_5 units
213.6	0.15	9	SeO_3 units vibrating against CuO_5 units
232.2	0.12		General motion of SeO_3 and CuO_5 units
277.9[a]	0.09		Vibration of SeO_3 units
289.2[a]	0.01		General motion of SeO_3 units
305.6	0.20		General motion of SeO_3 units
317.8	0.23	13	Internal in-plane vibration of CuO_5 units
374.3	0.57		Internal in-plane vibration of CuO_5 units
386.7	1.85	14	Internal bending mode of SeO_3 units
401.3	0.35		General motion of CuO_5 units
408.9	0.71		General motion of CuO_5 units
412.0	0.80		General motion of CuO_5 units
423.8	0.70		Internal out-of-plane vibration of CuO_5 units
435.3	0.73	16	Internal out-of-plane vibration of CuO_5 units
444.4	0.90		General motion of Oxygen atoms
450.2[c]	0.22		General motion of Oxygen atoms
453.3[c]	0.63		General motion of Oxygen atoms
469.0[a]	0.07		General motion of Oxygen atoms
485.6[a]	0.06		General motion of Oxygen atoms
492.1	0.24		General motion of Oxygen atoms
498.7	0.43		General motion of Oxygen atoms
512.6	0.68		Internal vibration of SeO_3 units
517.7	0.49		General motion of Oxygen atoms
525.5	0.17		General motion of Oxygen atoms
557.4	0.46		General motion of Oxygen atoms
716.2	1.30	22	Antisymmetric stretch of SeO_3 units
750.7	0.56		General motion of SeO_3 units
782.4[c]	0.83	24	Antisymmetric stretch of SeO_3 units
790.0[c]	0.57		Antisymmetric stretch of SeO_3 units
803.3	0.34		General motion of SeO_3 units
830.7	0.30	26	Radial breathing mode of SeO_3 units

[a]Possibly not resolved because of merging due to weak dipole moments on adjacent phonons.
[b]The phrase "general motion" refers to modes where the atoms or units in motion are known, but the specific nature of the motion is unclear.
[c]Possibly not resolved because of merging phonons due to broad linewidth of an experimentally observed phonon.

served that anomalous behavior usually could be found in all three oscillator parameters.

C. Assignment of phonon modes

Because the magnetodielectric effect is observed through lattice dynamics, we make a partial analysis of the phonon spectrum. The number of phonon modes expected in Cu_2OSeO_3 can be found by space-group analysis. Using the SMODES program,[15] we arrive at the following distribution of modes:

$$\Gamma^{optical} = 14A^{(R)} + 14E^{*(R)} + 41T^{(R,IR)}, \quad (3)$$

where (R) and (IR) denote Raman active and infrared active modes, respectively. We therefore have the potential of 41 total infrared active modes, all of which possess threefold degeneracy as indicated by their irreducible representation. However, only 26 modes in the infrared spectrum are detected. The oscillator parameters (at 20 K) of the 26 experimentally observed modes are listed in Table I. Based on our lattice dynamical calculation of the position of the 41 predicted modes and the experimental linewidth of the 26 observed modes, we suspect that weaker phonons are buried within stronger phonons and merge in the spectrum. The Lorentz analysis for merged phonons would result in an average of oscillator parameters weighted by oscillator strength.

More specifically, the lattice dynamical calculation employed herein are based on a real-space summation of screened coulomb interactions involving a spherical cut-off boundary.[16] Frequency, mode intensity, as well as displacement pattern were calculated based on the structure and valence as reported by Bos *et al.*[9] The center frequency, mode intensity, and specific nature of atomic vibration of all calculated modes are listed in Table II. We have indicated groups of the calculated modes where a potential merging may have occurred in the experimental spectra. We were also able to assign eight strong modes in the infrared spectrum by comparing the calculated and experimental spectra.

Table I details the mode assignments made using the adopted numbering scheme and center frequency of each oscillator for identification. In addition, we have distinguished between oscillators exhibiting anomalous behavior in one parameter (type A), two parameters (type B), and all three parameters (type C). It should be noted that oscillators #13 and #16, which exhibit anomalous behavior at the transition temperature in all three oscillator parameters (#13 is shown in Fig. 8), are associated with vibrations of oxygen around the central copper, the ion responsible for magnetic ordering.

V. CONCLUSIONS

Far-infrared measurements of single-crystal reflectance from Cu_2OSeO_3 reveal no drastic anomalies in the phonon spectrum at the ferrimagnetic transition temperature. However, a closer inspection of the dynamics of the phonon spectrum, as modeled through Drude-Lorentz fitting, uncover an anomalous jump in the dielectric constant near T_c. It is observed that 13 of the 28 total far-infrared phonons contribute to this magnetodielectric effect. A few strong far-infrared phonons have been assigned to motion of the CuO_5 and SeO_3 units via a lattice dynamical calculation. It is worth noting that two of the 13 modes exhibiting anomalous behavior across T_c have been assigned to the motions of oxygen around the central copper, the ion responsible for magnetic ordering. A weak phonon that was not resolved in reflectance is observed below 120 K in the transmission spectrum. A magnetic origin for this structure has yet to be ruled out.

Our infrared results agree with the Raman studies of Gnezdilov *et al.*[10] in that we also observed a number of phonon modes that exhibit anomalies in their strength, center frequency, or linewidth, but we differ on other issues. For example, we do not observe any new modes below the magnetic transition whereas Gnezdilov *et al.*[10] do detect some additional (rather weak and broad) features. They report three new modes appearing in the Raman spectra below the transition temperature at frequencies of ~261, 270, and 420 cm^{-1}. The only structure we observe in these three spectral regions is at 270 cm^{-1}, where one of the 13 reported anomalous phonons is present. The absence of a typical mode at 420 cm^{-1} gives further support to the claim by Genzdilov *et al.* that the new line appearing in their spectra at this frequency "unambiguously has magnetic origin." Genzdilov *et al.*[10] also reported two new lines originating below 20 K in the Raman spectra at ~86 and 203 cm^{-1}. Our infrared studies reveal a strong rather typical mode at ~86 cm^{-1} and a weak anomalous mode at 203 cm^{-1}. We have assigned the typical mode at ~86 cm^{-1} to the collective vibration of the edge-sharing CuO_5 units. If any new infrared features possessed the same relative intensities as reported for the Raman spectra, we would have observed them clearly.

ACKNOWLEDGMENTS

The authors wish to thank H. T. Stokes and F. Pfuner for valuable discussions on the SMODES program. This work was supported by DOE through Grant No. DE-FG02-02ER45984 and the NSF via Grant No. DMR-0701400.

[1] N. Hur, S. Park, P. A. Sharma, J. S. Ahn, S. Guha, and S.-W. Cheong, Nature (London) **429**, 392 (2004).
[2] C. Zhong, J. Fang, and Q. Jiang, J. Phys.: Condens. Matter **16**, 9059 (2004).
[3] T. Katsufuji and H. Takagi, Phys. Rev. B **64**, 054415 (2001).
[4] N. A. Hill, J. Phys. Chem. B **104**, 6694 (2000).
[5] S.-W. Cheong and M. Mostovoy, Nature Mater. **6**, 13 (2007).
[6] L. C. Chapon, G. R. Blake, M. J. Gutmann, S. Park, N. Hur, P. G. Radaelli, and S.-W. Cheong, Phys. Rev. Lett. **93**, 177402 (2004).
[7] C. R. dela Cruz, F. Yen, B. Lorenz, M. M. Gospodinov, C. W. Chu, W. Ratcliff, J. W. Lynn, S. Park, and S.-W. Cheong, Phys.

Rev. B **73**, 100406 (2006).
[8] E. Montanari, G. Calestani, L. Righi, E. Gilioli, F. Bolzoni, K. S. Knight, and P. G. Radaelli, Phys. Rev. B **75**, 220101 (2007).
[9] Jan-Willem G. Bos, C. V. Colin, and T. T. M. Palstra, Phys. Rev. B **78**, 094416 (2008).
[10] V. Gnezdilov, K. Lamonova, Y. Pashkevich, P. Lemmens, H. Berger, F. Bussy, and S. Gnatchenko, Fiz. Nizk. Temp. **36**, 688 (2010).
[11] H. Effenberger and F. Pertlik, Monatsch. Chem. **117**, 887 (1986).
[12] M. Kobets, K. Dergachev, E. Khatsko, A. Rykova, P. Lemmens, D. Wulferding, and H. Berger, J. Low Temp. Phys. **39**, 176 (2010).
[13] A. Larrañaga, J. Mesa, L. Lezama, J. Pizarro, M. Arriortua, and T. Rojo, Mater. Res. Bull. **44**, 1 (2009).
[14] F. Wooten, *Optical Properties of Solids* (Academic Press, New York, 1972).
[15] H. T. Stokes and D. M. Hatch, 1999, SMODES, www.physics.byu.edu/stokesh/isotropy.html
[16] D. Wolf, P. Keblinski, S. R. Phillpot, and J. Eggebrecht, J. Phys. Chem. **110**, 8254 (1999).
[17] M. Belasi, I. Rousochatzakis, H. C. Wu, H. Berger, I. V. Shvets, F. Mila, and J. P. Ansermet, Phys. Rev. B **82**, 094422 (2010).